Shape Derivative Adapted to Elastodynamics for the Reconstruction of Corrosion Defects

AXEL THOMAS, TOM DRUET, ARNAUD RECOQUILLAY and BASTIEN CHAPUIS

ABSTRACT

Today, the residual thickness of a structure is crucial information for many industries, including the nuclear sector. To this end Structural Health Monitoring (SHM) aims to establish continuous monitoring using sensors integrated into the structure to be inspected. We are particularly interested in tomographic methods using guided elastic waves.

In the literature, the most widely studied guided elastic wave tomography methods are based on an acoustic propagation model. These methods are based on physical approximations, such as single-mode propagation or propagation in a waveguide-type structure, which allow a rapid estimation of the thickness. However, these assumptions are only valid if the wave packet of interest can be extracted from the rest of the signal and there is no mode conversion at the defects, as this would inevitably affect imaging resolution and potential application cases.

We present here an adaptation of a method called 'shape derivative' that does not rely on these assumptions.

Axel Thomas, University of Paris Saclay, CEA List, F-91120 Palaiseau, France
Tom Druet, University of Paris Saclay, CEA List, F-91120 Palaiseau, France
Arnaud Recoquillay, University of Paris Saclay, CEA List, F-91120 Palaiseau, France
Bastien Chapuis, University of Paris Saclay, CEA List, F-91120 Palaiseau, France

INTRODUCTION

Today, the residual thickness of a structure subjected for example to corrosion is a crucial information for many industries, including the nuclear sector. To this end Structural Health Monitoring (SHM) aims to establish continuous monitoring using sensors integrated into the structure to be inspected. We are particularly interested in tomographic methods using guided elastic waves.

In the literature, the most widely studied guided elastic wave tomography methods are based on an acoustic propagation model [1]. These methods are based on physical approximations, such as single-mode propagation or propagation in a waveguide-type structure, which allow a rapid estimation of the thickness. However, these assumptions are only valid if the wave packet of interest can be extracted from the rest of the signal and there is no mode conversion at the defects, as this would inevitably affect imaging resolution and potential application cases. In practice, it has been shown that the resolution of this type of algorithm on an elastic signal is close to 1.5λ to 2λ [2], where λ is the wavelength of the used guided mode, and as expected, the results deteriorate as one moves away from perfect waveguide.

There are also algorithms that take the full waveform into account, namely the Full Waveform Inversion (FWI) method [3, 4]. However, for SHM applications, these algorithms have mainly been applied to the acoustic case in order to reduce the computational load but not fully alleviating limitations of conventional methods.

To overcome these limitations, we study in this paper a FWI tomography method based on equations of elastodynamics and mesh deformation techniques, similarly as in the work described in [5]. However, in our case, we use a technique called “shape derivative” to optimise a deformation of the mesh representative to corrosion (loss of thickness) shape. Shape derivative is an iterative method that solves the inverse problem of optimal shape, widely studied in the context of continuum mechanics, for example [6]. The objective is to identify the optimal shape of a structure subjected to a given stress while minimising a certain criterion. One example is maximising stiffness for a given volume. In our case, the functional is established as the difference between experimental data and simulated signals, and the control surface is the profile of the structure subjected to corrosion. Simulated signals are obtained by solving the equations using the finite element method and a mesh of the structure under study. Considering, in our case, the equations of motion of elastodynamics, the limits previously considered in the acoustic case should be attenuated. This makes possible to take better account of the real structure and therefore to increase the resolution and the possible use cases compared with tomography algorithms based on an acoustic model. Compared to [5] no geometric parameterisation of the defect is necessary, which eliminates the need to make assumptions about defect position or geometry.

Our solution uses spectral finite elements to solve the direct problems required at each iteration. This allows the method to be applied to generic structures with a limited computational load compared with traditional finite element methods. However, even using the spectral finite element method, the computation time remains significant. Especially since the elastodynamic system has to be solved several times per iteration. To overcome this limitation, we decided to use the results of acoustic tomography by guided waves as the first estimate of the thickness of the structure [7]. This allows to reduce the number of iterations and limit convergence to local minima due to the smaller distance to the true solution.

This paper begins by describing the method used. We will then show how the initial acoustic estimate saves calculation time. Finally, we show how the use of a first estimate overcomes the problem of convergence towards local minima in practice.

SHAPE DERIVATIVE TOMOGRAPHY

The mathematical problem is an adaptation of static shape derivative described in [6] and adapted to the dynamic case. We consider a reference regular open bounded domain Ω_0. The boundary variation method creates a domain sequence of the form $\Omega_\theta := (1 + \boldsymbol{\theta})\,\Omega$, where Ω is a given domain and θ a mathematical object that represents a vector field used to update the domain. In order to obtain the medium response to the propagation of guided waves, we need to solve the elastodynamic system defined such as $\boldsymbol{u}(\boldsymbol{x},t)$ satisfies:

$$\begin{cases} \rho(\boldsymbol{x})\partial_{tt}\boldsymbol{u}(\boldsymbol{x},t) - \nabla\cdot\boldsymbol{\sigma}\big(\boldsymbol{u}(\boldsymbol{x},t)\big) = 0 & \text{in } \Omega\times[0,T] \\ \boldsymbol{\sigma}\big(\boldsymbol{u}(\boldsymbol{x},t)\big)\cdot\boldsymbol{n} = g(\boldsymbol{x},t) & \text{on } \Gamma \times[0,T] \\ \boldsymbol{u}(\boldsymbol{x},t) = \partial_t\boldsymbol{u}(\boldsymbol{x},t) = 0 & \text{on } \Omega\times\{0\} \end{cases} \tag{1}$$

where $\boldsymbol{\sigma}(\boldsymbol{u}) = \boldsymbol{C}:\boldsymbol{\varepsilon}(\boldsymbol{u})$, $\rho(\boldsymbol{x})$ is the density, $\boldsymbol{n}$ is the normal oriented outside the domain, $g(\boldsymbol{x},t)$ is the surface load, Γ is the boundary.

The spectral finite element solver of SHM module in CIVA software is used [8, 9, 10]. This solver is based on an explicit leapfrog scheme in time and high-order spectral finite elements in space. Compared to the traditional finite element method, the spectral finite elements method leads to mass lumping. The linear system then relies on the inversion of a diagonal mass matrix and a stiffness matrix which does not need to be assembled. Thus, the application at each time step has a very small computational cost and memory usage.

To define our inverse problem, we used a least-square minimization framework. The associated L_2 shape derivative cost function is formulated as:

$$J(\Omega) = \sum_{0}^{N} \frac{1}{2}\iint_{\partial\Omega\times[0,T]} \|\boldsymbol{d}\boldsymbol{u}_\Omega - \boldsymbol{u}_{obs}\|^2 \,\mathrm{d}x\,\mathrm{d}t \tag{2}$$

where $\boldsymbol{u}_\Omega$ and $\boldsymbol{u}_{obs}$ are, respectively, the elastic displacement resulting from the resolution of (1) and the measured displacement, N the number of sensors pairs and $\boldsymbol{d}$ the observation function which extracts the part of the solution u_Ω corresponding to the measurement. Finally, the adjoint state method is used to compute the associated gradient of (2) with respect to the shape. It is expressed as:

$$\nabla J(\Omega)(\boldsymbol{\theta}) = -\iint_{\partial\Omega\times[0,T]} \boldsymbol{\theta}.\boldsymbol{n}\big(\rho\boldsymbol{v}\partial_{tt}\boldsymbol{u} + \boldsymbol{\varepsilon}(\boldsymbol{u}):\boldsymbol{C}:\boldsymbol{\varepsilon}(\boldsymbol{v})\big)ds\,\mathrm{d}t \tag{3}$$

where $\boldsymbol{v}$ is the adjoint variable that represents the elastic displacement obtained by solving the elastodynamic adjoint formulation [11, 12]. As (1) is self-adjoint, the formulation of its adjoint state is identical, but with a different source term. However, to maintain the symmetry in the adjoint operator, the initial condition in (1) becomes a final condition in the adjoint formulation, making it unsolvable directly. Therefore, the

equation is computed in inverse time, and the result is obtained in time due to the reversibility property of waves. According to (3), we see that the gradient only depends on the normal component of the boundary, this means that the surface is moved in the opposite direction to the gradient, leading to a reconstruction of the domain thickness. In practice, this step involves moving the vertices of the mesh along the $\boldsymbol{\theta}.\boldsymbol{n}$ vector at each iteration. The next iteration is then computed on the updated domain Ω_θ and repeated accordingly. The shape of the domain represents the optimization variable of the problem through its discretization.

The quasi-Newton methods, namely BFGS, linked to the Armijo criterion are used to compute a descent direction from the value of the computed gradient (3) and an adapted descent step α, enabling rapid and robust convergence [13]. An acoustic diffraction tomography was used [7] to perform the domain thickness initialization. By an arbitrary choice, at the first step α is chosen as a percentage of plate thickness.

RESULTS

After presenting the experimental set-up used to acquire the data this section will present two significant results. Firstly, we will demonstrate the value of using an a priori to initialize the algorithm by showing an initial experimental result. Then, we will address the problem of convergence to local minima and explain how initialization can be used to solve it.

We are interested here in the experimental data from a previous study, see [14]. The physical measurements were taken from a corroded aluminium plate of size 600×580×3 mm^3 instrumented with 48 PZT transducers of radius $r_{PZT} = 5$ mm according to a circular distribution of radius $r_{distrib}$ = 150 mm, see Figure 1. The acquisition sequence is a Round Robin acquisition, i.e. that each PZT is a transmitter in turn while the others are receivers. This is the advantage of PZT transducers: they can be used as both transmitters and receivers of guided waves. The transmitted signals are 5-cycles tone burst with a centre frequency f = 40 kHz. Each sensor acquires a 1 ms signal with a sampling frequency of 2 MHz. To simulate corrosion/metal erosion, an EDM process was used. This process was chosen for its ability to create defects similar to a real corrosion defect. In this article, we will focus on two stages of corrosion. An acquisition was carried out for each of them. The smallest defect is an ellipse with a depth of 1.1 mm, see Figure 2a, and the largest defect is a circle with a depth of 1.5 mm, i.e. half the thickness of the plate, see Figure 4a.

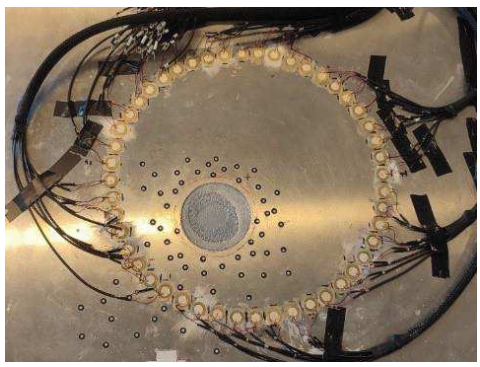

Figure 1: Experimental setup.

Acoustic initialization

As mentioned previously, providing the results of the acoustic algorithm as the first estimate should reduce the number of iterations before convergence and help converge to the true solution by reducing the convergence to local minima.

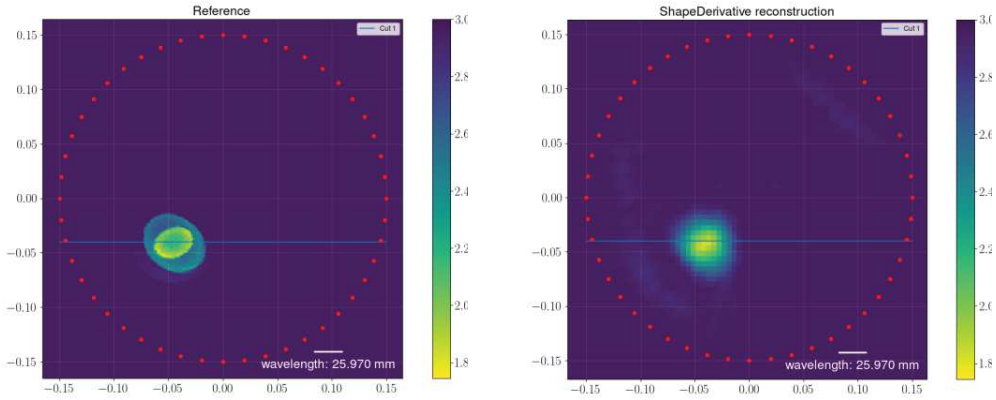

(a) Reference thickness map (b) Shape derivative reconstruction

Figure 2: Case 1: Shallow corrosion.

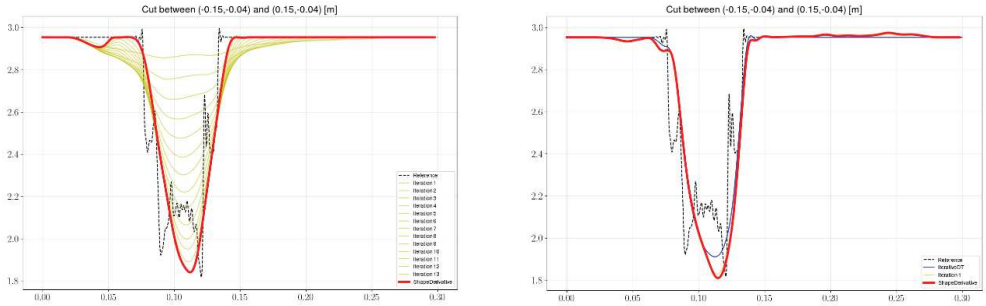

(a) without tomography initialization (b) with initialization

Figure 3: Horizontal cross-section of shape derivative result presented in Figure 2b.

Figure 2a shows the reference thickness mapping from this study obtained with a structured light 3D scanner (Go Scan®) while Figure 2b shows the reconstruction using the shape derivative algorithm. In addition, there is a cross-section of the reconstructed thickness, plotted in Figure 3a. The red line represents the result of the shape derivative at convergence, the yellow lines represent the successive iterations and the dotted black line represents the reference. From the reconstruction shown in Figure 2b, it can be seen that the defect is well positioned on the mapping. A closer look at the thickness cross-sections shows that the position, size and residual thickness of the defect have been correctly estimated, see Figure 3a. However, in the case without tomography initialization, convergence is reached after fifteen iterations, which takes several days on an Intel® Xeon® Silver 4216 @2.10GHz machine with 182GB Ram. Consequently,

the study is repeated using this time the result of the acoustic algorithm as first estimate. The same cross-section as for the case without initialization is plotted in Figure 3b.

The blue line represents the result of the acoustic tomography algorithm and the red line represents the result of the shape derivative algorithm when the initial estimate of the domain is given by the blue curve. Note that convergence is achieved after only two iterations of the "elastic" shape derivative instead of 13 with no initialisation, which represents a significant reduction of computation time. In addition, the thickness is slightly better estimated and the background of the image is less noisy. So, as Figure 3 shows, adding an a priori calculated by acoustic tomography makes it possible to solve the computation time issues outlined above. Let's now consider a specific case of convergence to a local minimum.

Convergence to a local minimum

We will now present the case of a deeper and wider corrosion fault. Figure 4a shows the thickness map for the case study in this section. The defect is half the healthy thickness deep and has a width of about 3λ. The result shown in Figure 5a is obtained using the shape derivative algorithm without initialization.

The cross-section would appear to show an excess thickness at the location of the defect, but this is not the case in reality. This is proof that the algorithm has converged to an incorrect solution, i.e. to a local minimum. As a result, convergence is halted after the first iteration. This is due to a common problem in inversion with ultrasound signals, known as "cycle skipping" [15]. Indeed, in the shape derivative approach, the L_2 functional is defined as the difference between the data and the simulated signals, as can be seen in (3). However, the signals are oscillating so when the difference between the signals is approximately equal to one period, the functional reaches a local minimum. To solve this problem, initialization can be an interesting option.

As the initial structure is closer to the solution, the value of the functional will be closer to the global minimum. Convergence towards it is therefore easier. Figure 5b shows the cross-section of the mapping obtained by shape derivative with the acoustic initialization. This time, the position, size and thickness are correctly estimated. The result is even better than the acoustic result (blue curve in Figure 5b). It should be noted that in the case of smooth defects such as those presented in this study, the acoustic algorithm performs very well. This demonstrates the greater accuracy obtained using the elastodynamic model. It has therefore been demonstrated that the coupling between acoustic and elastic tomography can be used to overcome the convergence problem. It can also be seen that in the case of the deep flaw, with an identical convergence criterion, the algorithm performs a greater number of iterations than in the case of the shallower fault. No conclusions can be drawn at this stage, but we might be interested in studying regularisations of the problem and a more robust estimate of the initial step.

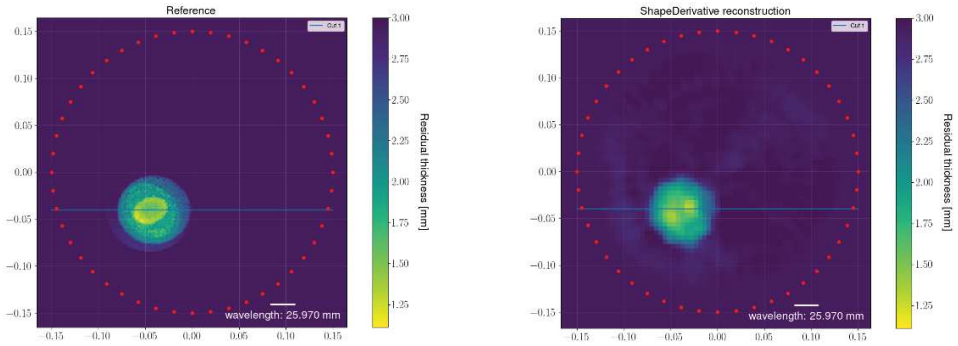

(a) Reference thickness map (b) Shape derivative reconstruction

Figure 4: Case 2: Deep corrosion.

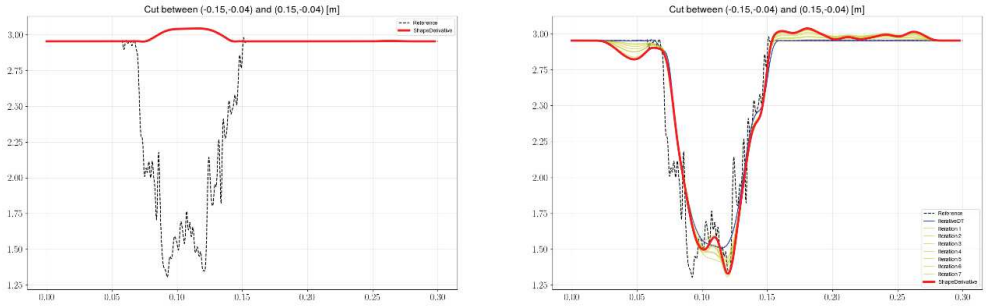

(a) without tomography initialization (b) with initialization

Figure 5: Horizontal cross-section of shape derivative result presented in Figure 4.

CONCLUSION

After a brief presentation of the development of the method, this paper demonstrates the application of the shape derivative in two experimental cases. First, it is shown that the initialization reduces the number of iterations required for convergence, which saves a significant amount of time. In addition, it also slightly improves the results. Secondly, it has been shown that initialization can help overcome the well-known local minima problem by bringing the functional closer to the solution. The next step will be to demonstrate the effectiveness of the method on more complex geometries, remote from a perfect waveguide, such as pipes with welded supports, which affect wave propagation.

ACKNOWLEDGMENTS

The authors would like to thank A. Imperiale for his considerable contribution in the context of the numerical solution of the wave problem and theoretical derivation of the method.

REFERENCES

1. Huthwaite, P., and F. Simonetti, 2011. “High-resolution imaging without iteration: a fast and robust method for breast ultrasound tomography,” The Journal of the Acoustical Society of America 130 (3), 1721–1734.
2. Huthwaite, P., 2014. “Evaluation of inversion approaches for guided wave thickness mapping,” Proceedings of the Royal Society A: Mathematical, Physical and Engineering Sciences 470 (2166), 20140063.
3. Rao, J., M. Ratassepp, and F. Zheng, 2016. “Guided Wave Tomography Based on Full Waveform Inversion,” IEEE Transactions on Ultrasonics, Ferroelectrics, and Frequency Control 63 (5), 737–745.
4. Operto, S., A. Gholami, et al., 2023. “Extending the search space of full-waveform inversion beyond the single-scattering Born approximation: A tutorial review,” Geophysics 88 (6), R671–R702.
5. Peng, Z., and P. Huthwaite, 2024. “Guided wave tomography for quantitative thickness mapping using non-dispersive SH0 mode through geometrical full waveform inversion (GFWI)”, Proc. R. Soc. A. 48020240132, http://doi.org/10.1098/rspa.2024.0132
6. Allaire, G., F. Jouve, and A.-M. Toader, 2004. “Structural Optimization using sensitivity analysis and a level-set method,” Journal of Computational Physics 194 (1), 363– 393.
7. Druet, T., J.-L. Tastet, B. Chapuis, and E. Moulin, 2019. “Autocalibration method for guided wave tomography with undersampled data,” Wave Motion 89, 265–283.
8. Imperiale, A., and E. Demaldent, 2019. “A microelement strategy based upon spectral finite elements and mortar elements for transient wave propagation modeling. Application to ultrasonic testing of laminate composite materials,” International Journal for Numerical Methods in Engineering 119 (10), 964–990.
9. “Structural Health Monitoring With CIVA,” URL: https://www.extende.com/structural-health-monitoring-with-civa (visited on May 15, 2025).
10. Mesnil, O., A. Recoquillay, T. Druet, V. Serey, T. Hoang, A. Imperiale, and E. Demaldent, 2021. “Experimental Validation of Transient Spectral Finite Element Simulation Tools Dedicated to Guided Wave-Based Structural Health Monitoring,” Journal of Nondestructive Evaluation, Diagnostics and Prognostics of Engineering Systems 4 (4).
11. Cea, J., 1986. “Conception optimale ou identification de formes, calcul rapide de la dérivée directionnelle de la fonction coût,” ESAIM : Modélisation mathématique et analyse numérique 20 (3), 371–402. URL: http://www.numdam.org/item/M2AN_1986__20_3_371_0/.
12. Plessix, R.-E., 2006. “A review of the adjoint-state method for computing the gradient of a functional with geophysical applications,” Geophysical Journal International 167 (2), 495–503.
13. Wright, S., J. Nocedal, et al., 1999. “Numerical Optimization,” Volume 35, Springer Science, 7.
14. Druet, T. A. Thomas, A. Recoquillay, Y. Gélébart, E. Martin, and B. Chapuis, 2023. "Guided Wave Tomography for Corrosion Monitoring under Varying Environmental Conditions," e-Journal of Nondestructive Testing, vol. 28, no. 7, doi: 10.58286/28283.
15. Engquist, B., and Y. Yang, 2021. "Optimal Transport Based Seismic Inversion: Beyond Cycle Skipping," Communications on Pure and Applied Mathematics, vol. 75, no. 10, pp. 2201–2244, doi: 10.1002/cpa.21990.